Journal of Solid State Chemistry 183 (2010) 684–691

Contents lists available at ScienceDirect

Journal of Solid State Chemistry

journal homepage: www.elsevier.com/locate/jssc

Mixed oxides of sodium, antimony (5+) and divalent metals (Ni, Co, Zn or Mg)

V.V. Politaev, V.B. Nalbandyan, A.A. Petrenko *, I.L. Shukaev, V.A. Volotchaev, B.S. Medvedev

South Federal University, 7 ul. Zorge, Rostov-na-Donu 344090, Russia

ARTICLE INFO

Article history:
Received 2 August 2009
Received in revised form
30 November 2009
Accepted 7 December 2009
Available online 16 December 2009

Keywords:
Antimonate
Superlattice
Ionic conductivity
α-$NaFeO_2$ type
Delafossite
Ion exchange
Rietveld
Stacking faults

ABSTRACT

A family of α-$NaFeO_2$-type oxides $Na_xM_{(1+x)/3}Sb_{(2-x)/3}O_2$ (M=Ni, Co, Zn, Mg; $x \approx 0.8$ or 0.9) has been prepared by solid state reactions and characterized by powder XRD. At x=1, ordering occurs with tripling the unit cells and formula units. The powder patterns for $Na_3M_2SbO_6$ (M=Ni, Co) comply with both trigonal $P3_112$ cell and monoclinic $C2/m$ cell. The Ni compound exhibits also a series of extremely weak reflections ($I < 0.3\%$) that need doubling of the c axis, and the final cell is $C2/c$, a=5.3048(3), b=9.1879(4), c=10.8356(7), β=99.390(5). These ambiguities are explained by stacking faults. The compounds absorb atmospheric moisture with c-axis expansion up to 29%. A delafossite-related superlattice $Ag_3Co_2SbO_6$ has been prepared by ion exchange and refined: $P3_112$, a=5.3842(2), c=18.6613(10). Ionic conductivity of the $Na_{0.8}Ni_{0.6}Sb_{0.4}O_2$ ceramics, 0.4 S/m at 300 °C, is greater than reported previously, presumably owing to the grain orientation produced by hot pressing.

1. Introduction

Mixed antimonates attracted our attention due to possible formation of layered phases with considerable mobility of alkali cations. With components easily changing their oxidation states, these phases may be useful electrode materials for electrochemical cells. With stable oxidation states, they may be interesting solid electrolytes. Recently, some of the present authors reported two new families of cation-conducting layered phases $K_xM_{(1+x)/3}Sb_{(2-x)/3}O_2$ (M=Ni, Co, Mg) [1], phase relations and crystal chemistry in Na_2O–Fe_2O_3–Sb_2O_5 [2] and Na_2O–CuO–Sb_2O_5 [3] systems. Phase transition, crystal structure and ionic conductivity of $Na_{0.8}Ni_{0.6}Sb_{0.4}O_2$ were also studied [4,5]. Preliminary data for systems Na_2O–MO–Sb_2O_5 (M=Mg^{2+}, Co^{2+} and Ni^{2+}) were reported in brief earlier [6–8] and X-ray diffraction (XRD) patterns of some compounds were included into the Powder Diffraction File (00-53-344, 00-54-1031, 00-58-134, 00-58-771). In particular, it has been shown that rhombohedral disordered phases $Na_xM^{2+}_{(1+x)/3}Sb_{(2-x)/3}O_2$ become ordered primitive trigonal when x approaches unity, i.e., $Na_3M_2SbO_6$. We describe here these systems with divalent cations, including M=Zn, in more detail. When the present work was close to completion, a paper on crystal structure and magnetic properties of $Na_3Co_2SbO_6$ appeared [9]. We discuss those results in parallel with ours. Magnetic properties and electronic structure of $Na_3Cu_2SbO_6$ were also investigated [10,11]. No other information on these quasi-ternary systems has been found in literature, whereas simple antimonates (5+) of sodium [12–14] and divalent metals [15–21] are well known. A trirutile-type phase MSb_2O_6 is present in each of the four systems MO–Sb_2O_5 (M=Mg, Co, Ni, Zn). For M=Ni, it is the only double oxide with Sb(5+), whereas M=Co and Zn give rise also to spinel-type phases $M_7Sb_2O_{12}$ (or $M_{7/3}Sb_{2/3}O_4$), and the MgO–Sb_2O_5 system contains a series of four MgO-enriched hexagonal phases, all having almost identical a-axes but different c-axes. Interestingly enough, $NaSbO_3$ [13] and $Mg_4Sb_2O_9$ [16], apparently of different formula types, belong both to the ilmenite family. The analogy between them becomes visible when the magnesium antimonate is rewritten as $Mg(Mg_{1/3}Sb_{2/3})O_3$.

2. Experimental

Starting materials were reagent-grade antimonic acid, sodium carbonate, sodium nitrate, hydrous nickel oxide and hydrous cobalt oxide and/or basic carbonates of magnesium, cobalt, nickel and zinc. Na_2CO_3 and $NaNO_3$ were dried for 2 h at 200 °C and other reagents were analysed gravimetrically for volatile components and then used as received. In some instances, presynthesised MSb_2O_6 were used as reagents. The main source of sodium was Na_2CO_3, but in some preparations it was partially substituted by

* Corresponding author.
E-mail addresses: aapetrenko@sfedu.ru, apetrenko@rsu.ru (A.A. Petrenko).

0022-4596/$ - see front matter © 2010 Elsevier Inc. All rights reserved.
doi:10.1016/j.jssc.2009.12.002

low-melting $NaNO_3$ to intensify the reaction. Weighed amounts of reagents were thoroughly mixed with a mortar and pestle, pressed and calcined in two or three steps, 1–3 h each, with intermediate regrinding and pressing, first at 630–850 °C to expel volatile components, and then at 1000–1200 °C. After the final heat treatment, the samples were air-quenched and studied by powder X-ray diffraction (XRD). Small sodium excess was introduced to compensate for high-temperature volatilisation; 3–10% excess was found adequate, in contrast to 20% [9], probably because each our pellet was surrounded with the powder of the same composition to reduce losses. The total weight of each composition was about 2–4 g; half of this was pressed and the rest was used as the packing powder.

XRD scans for phase analysis were performed in Ni-filtered Cu$K\alpha$ radiation with a DRON-2.0 diffractometer. Higher-quality patterns for structural studies were measured using Rigaku D/Max B or D/Max-RC instruments equipped with secondary-beam graphite monochromators, also in copper radiation. Corundum powder (NIST SRM 676) served as an internal standard assuming a=4.7592 Å, c=12.9920 Å. To reduce grain orientation, amorphous low-attenuating materials (coffee or beryllium carbonate) were admixed. Cell constants were refined with CELREF3 (J. Laugier, B. Bochu). Rietveld profile analysis was performed using GSAS+EXPGUI suite [22,23].

For determination of silver content in the ion-exchange product, the samples were dissolved in hot sulphuric acid and the diluted cool solutions were titrated with thiocyanate.

Ceramic samples were prepared by hot pressing at 1100 °C and 40 MPa. The green compacts were surrounded with coarse-grained alumina. After the hot pressing, the contaminated outer layers of ceramics were removed with a diamond saw. Phase purity and grain orientation were studied by XRD, and only a single-phase sample was used for conductivity measurements. Opposite faces of the parallelepiped-shaped sample were electroded with graphite, and impedance was measured in the frequency range 10 Hz–200 KHz at constant temperatures using an original immittance analyser developed in the Institute of Control Sciences, Russian Academy of Sciences, Moscow. Electronic contribution to the total conductivity was roughly estimated by low-voltage dc measurements and found negligible ($<1\%$).

3. Results and discussion

3.1. Quasiternary systems Na_2O–MO–Sb_2O_y (M=Ni, Co, Zn, Mg)

It is known from the cited literature and confirmed in this work that Sb(5+) is stabilized in presence of basic oxides (Na_2O and/or MO), even at high temperatures, and its volatility at 1000–1100 °C is negligible, in contrast to free Sb_2O_y. Lower-valence Sb compounds appear only in compositions with >50 mole % Sb_2O_y. The systems with M=Ni and Zn were studied in more detail. Besides abovementioned layered phases, structurally related to α-$NaFeO_2$, no other triple oxides have been found within $NaSb_3O_7$–Na_3SbO_4–MO–MSb_2O_6 quadrangles. However, possibility of narrow solid-solution regions based on double oxides cannot be excluded. The system with M=Ni contains also a high-temperature hexagonal phase (P2-type), but it only could be quenched using liquid nitrogen [5] and did not appear in the air-quenched samples discussed here.

$Na_xNi_{(1+x)/3}Sb_{(2-x)/3}O_2$ compositions in the vicinity of x=0.8 have α-$NaFeO_2$-type structure with disordered arrangement of Ni and Sb on octahedral sites [4–8]. However, with x approaching unity and Sb:Ni ratio approaching a rational value of 1:2, a set of superlattice reflections appears, indicating formation of an ordered phase $Na_3Ni_2SbO_6$ with tripled formula volume (Fig. 1).

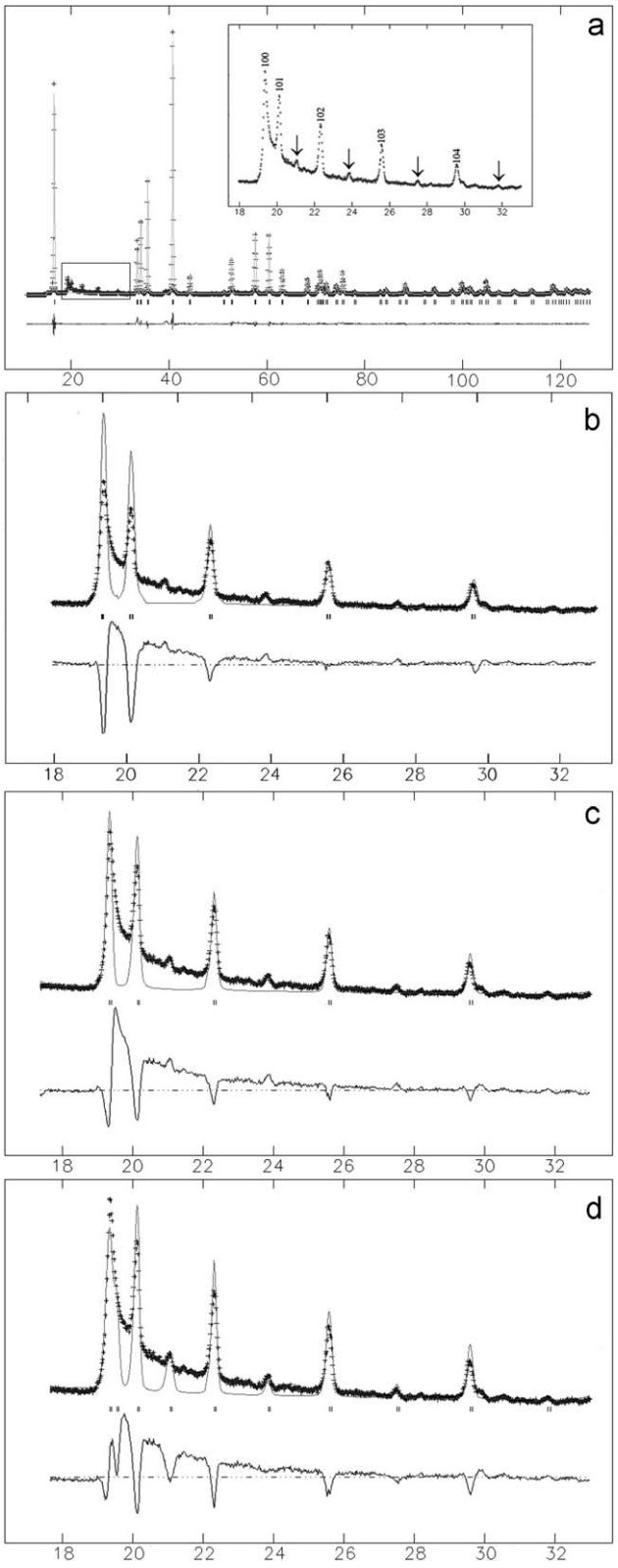

Fig. 1. X-ray diffraction pattern of $Na_3Ni_2SbO_6$: (a) General view and results of Rietveld refinement in the R-3m subcell, region $18^\circ < 2\Theta < 32^\circ$ omitted. This region, expanded, is shown in the insert with hkl's referring to the $P3_112$ supercell and arrows pointing to additional reflections not explained by $P3_112$ or $C2/m$ models, with half-integer l values (1 0 3/2, 1 0 5/2, 1 0 7/2 and 1 0 9/2). (b), (c), (d) Results of Rietveld refinement in $P3_112$, $C2/m$ and $C2/c$ supercells, respectively, in the region with the strongest superlattice reflections. Crosses, experimental data; line, calculated profile; bottom, difference profile; vertical bars, Bragg positions.

Its structure is discussed in Section 3.2. Excepting these weak reflections, both XRD patterns are very similar. For the disordered α-$NaFeO_2$ type, designation O3 is widely adopted, where O stands for octahedral (rather than prismatic, P) coordination of sodium and 3 indicates the number of layers in the hexagonal unit cell. The ordered variant will be designated O3S (S=superlattice). These two structure types appear in all the four systems (M=Ni, Co, Zn, Mg), but no analogue with M=Mn could be prepared so far. Their XRD patterns are very similar to that of Fig. 1 (two examples are shown in Fig. 2), with small variations in (sub)cell volumes showing a reasonable correlation with ionic radii [24] of M^{2+} (Table 1). The disordered phase with M=Zn differs from others by somewhat greater x value, ca. 0.9. At x=0.89, weak reflections from $NaSbO_3$ are visible, and at x=0.92, distinct superlattice reflections appear.

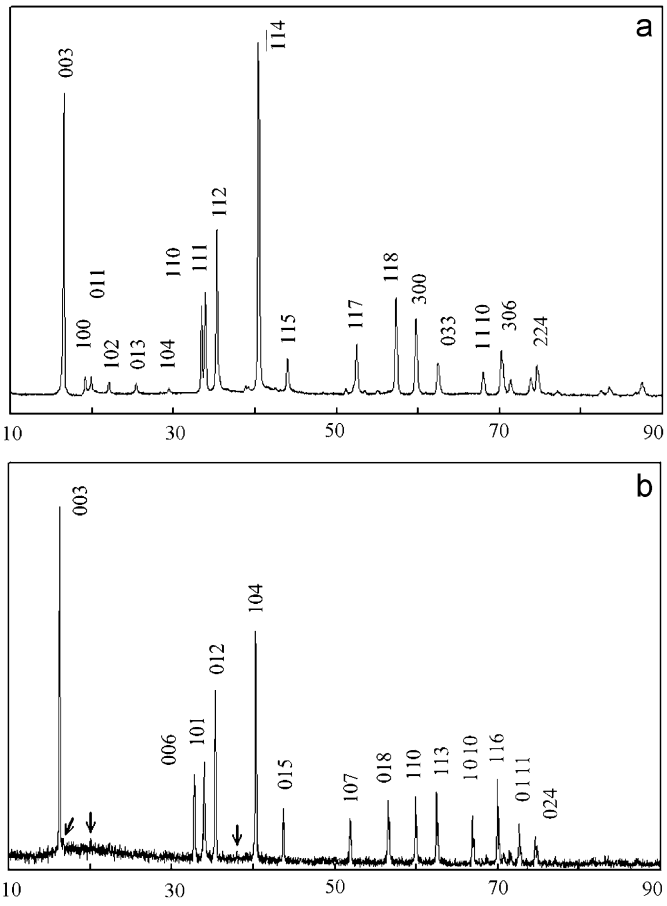

Fig. 2. X-ray diffraction patterns of $Na_3Co_2SbO_6$ (a) and $Na_{0.89}Zn_{0.63}Sb_{0.37}O_2$ (b).

Compounds with Ni are light green, those with Co are pink and others are white. In the systems $Na_xM_{(1+x)/3}Sb_{(2-x)/3}O_2$ (M=Co, Mg) at x values lower than ~0.8, the O3 phases coexist with $NaSbO_3$ and MgO or Co_3O_4; other phase triangles have not been studied and possible existence of other compounds cannot be excluded. With M=Mg, the synthesis was kinetically hindered, and the new compounds prepared at 1100 °C always contained impurity phases. Thus, their compositions could not be established accurately. Equilibration of the MgO-containing samples needs much higher temperatures where volatilisation of antimony oxides becomes unavoidable [16].

It should be noted that Cava et al. [9] prepared $Na_3Co_2SbO_6$ under entirely different conditions: 2 days at 800 °C in nitrogen atmosphere with 20% excess Na_2CO_3, in contrast to our 3 h at 1050 °C in air with 4% excess Na_2CO_3. Nevertheless, lattice constants from both sources agree very well, within 0.02–0.06% (Table 2). This means that compositions of the two preparations are identical, because small admixtures of Co^{3+} (due to oxidation in air) or Sb^{3+} (due to loss of oxygen in inert atmosphere) must drastically affect lattice parameters. In addition, mixed valence (Co^{2+}/Co^{3+}) usually produces dark coloration, not observed with our samples.

Table 1 and Fig. 3 also show that, similarly to layered $Na_x(M_yTi_{1-y})O_2$ [25–29] and $K_xM_{(1+x)/3}Sb_{(2-x)/3}O_2$ [1] systems, decrease in x causes c-axis expansion, because of interlayer O–O repulsion near alkali ion vacancies, and contraction in the (001) plane due to smaller ionic size of Sb(5+) compared to those of M^{2+}. Comparison of the formula volumes (Table 1) demonstrates that the former effect is stronger. The changes are not large, and it is difficult to distinguish between solid solutions and two-phase mixtures in the intermediate regions, $0.8 < x < 1$. Careful examination of two XRD patterns, $Na_xNi_{(1+x)/3}Sb_{(2-x)/3}O_2$ (x=0.85 and 0.9), still shows that reflections with large values of index l (1,0,10; 0,0,12; 1,1,12) are split. This indicates presence of two phases with different c values (Fig. 3). Reflections with small or zero index l are not split in the same samples, since relative changes in a is much smaller than changes in c. Thus, instead of two separate and constant a-axis values in the heterogeneous region, we only obtain an averaged value changing monotonically. Similar two-phase regions may be anticipated (although not detected experimentally) in the three other systems.

In another heterogeneous region of Fig. 3, O3+$NaSbO_3$+NiO ($x < 0.79$), lattice parameters are not constant, too. This may be explained by somewhat different conditions of quenching. As reported previously [5], above ca. 1000 °C a P2-type phase exists. Quenching in air cannot prevent P2→O3 transformation and, depending of the cooling rate, more or less $NaSbO_3$+NiO are precipitated from the O3 phase to increase its x value. Obviously,

Table 1
Comparison of hexagonal lattice parameters and volumes (per $A_x(M,Sb)O_2$ formula unit) for mixed sodium (or silver) divalent metal antimonates.

Composition	a (Å)	c (Å)	$^{VI}R(M^{2+})$ (Å) [24]	V (Å^3)
$Na_{0.8}Ni_{0.6}Sb_{0.4}O_2$ [4]	3.0496(1)	16.4060(4)	0.83	44.05
$Na_3Ni_2SbO_6$[a]	5.3046(9)=3.0626 × √3	16.0365(5)		43.42
$Na_3Mg_2SbO_6$[b]	5.317(4)=3.070 × √3	16.19(1)	0.86	44.0
$Na_3Cu_2SbO_6$ [3]	Monoclinic		0.87	44.82
$Na_{0.89}Zn_{0.63}Sb_{0.37}O_2$	3.0870(6)	16.40(2)	0.88	45.12
$Na_3Zn_2SbO_6$	5.3552(17)=3.0918 × √3	16.1510(2)		44.57
$Na_{0.8}Co_{0.6}Sb_{0.4}O_2$	3.0663(16)	16.4423(3)	0.885	44.63
$Na_3Co_2SbO_6$[a]	5.3576(7)=3.0932 × √3	16.0733(11)		44.39
$Ag_3Co_2SbO_6$	5.3820(17)=3.1073 × √3	18.6675(1)		52.03

[a] See Table 2 for more detail.
[b] The sample contained minor impurity phases.

Table 2
Variants of indexing powder patterns of $Na_3Co_2SbO_6$ and $Na_3Ni_2SbO_6$ and corresponding figures of merit FoM.

Symmetry and approach	a (Å)	b (Å)	c (Å)	β	FoM [36]	$b/a\sqrt{3}$	$(-3c\cos\beta)/a$
$Na_3Co_2SbO_6$ (5–100° 2Θ, 38 reflections)							
R-3*m* subcell: 25 reflections (26 *hkl*) including all strong and higher-angle reflections	3.0932(4)		16.0733(11)		F_{25}=67.3		
The same, tripled, $P3_112$ (all 38 reflections, 56 *hkl*)	5.3576		16.0733		F_{30}=25.7		
The same, transformed to *C*2/*m*	5.3576	9.2796	5.6476	108.434		1	1
Parameters refined in *C*2/*m*	5.3627(21)	9.2790(11)	5.6514(18)	108.55(4)	F_{30}=21.3	0.9990	1.0058
*C*2/*m* according to neutron data [9]	5.3681(2)	9.2849(4)	5.6537(2)	108.506(4)	?	0.9986	1.0029
$Na_3Ni_2SbO_6$ (10–126° 2Θ, 72 reflections)							
R-3*m* subcell: 41 reflections including all strong and higher-angle reflections	3.0626(5)		16.0365(5)		F_{30}=125		
The same, tripled, $P3_112$ (66 reflections)	5.3046		16.0365		F_{30}=37.7		
The same, transformed to *C*2/*m*	5.3046	9.1878	5.6304	108.303		1	1
Parameters refined in *C*2/*m*	5.3048(4)	9.1876(6)	5.6298(5)	108.300(5)	F_{30}=36.0	0.9999	0.9997
R-3*m* transformed to *C*2/*c* (all 72 reflections)	5.3046	9.1878	10.8362	99.390		1	1
Parameters refined in *C*2/*c*	5.3048(3)	9.1879(4)	10.8356(7)	99.390(5)	F_{30}=33.9	1.0000	0.9998

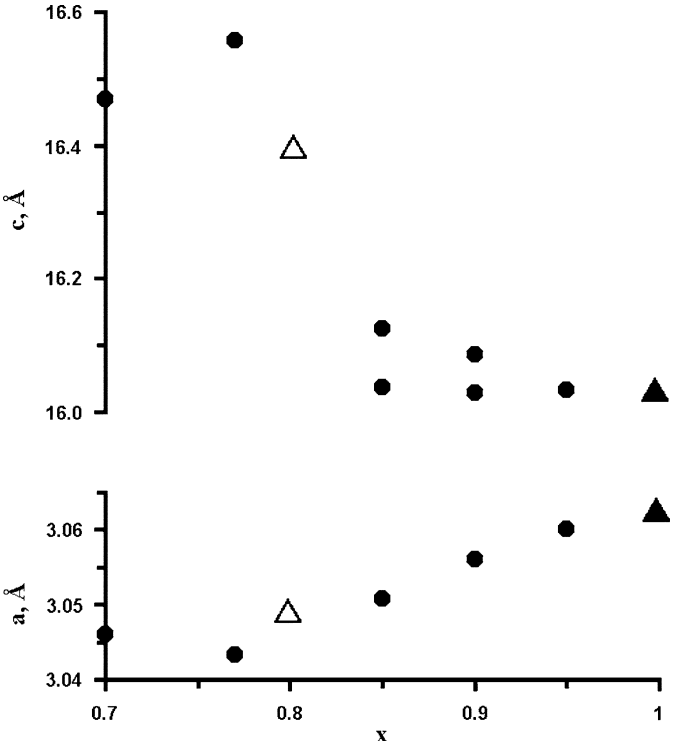

Fig. 3. Parameters of hexagonal (sub)cells in the system $Na_xNi_{(1+x)/3}Sb_{(2-x)/3}O_2$. Triangles, single-phase samples; circles, mixed-phase samples: NiO+$NaSbO_3$+O3 at $0.5<x<\sim0.79$ and O3+O3S at $\sim0.83<x<1$. See text for comments.

the sample having extreme parameters (that with nominal x=0.77) was quenched best and had the lowest x value of the O3 phase. The homogeneity range is, thus, very narrow, between $x\approx0.79$ and $x\approx0.83$ with uncertainty of about 0.02 determined by uncontrolled soda volatilisation, cooling rate and sensitivity of the XRD phase analysis.

Relative stability of layered phases with octahedral and prismatic coordination of alkali cation (O3 and P2 or P3) is of great interest due to higher ionic conductivity of prismatic phases. To distinguish between stability regions of these types, Hagenmuller et al. [30] proposed a diagram based on bond ionicity. According to it, $Na_xM_{(1+x)/3}Sb_{(2-x)/3}O_2$ systems should contain stable P2-type phases and $Na_x(M_yTi_{1-y})O_2$ (M=Ni, Co, Cr, Li) systems [25–29] should not, but the experimental results are exactly opposite. As indicated previously [7,27,28], the main reason for destabilizing O3 structure in favour of P2 (or P3) is strong alkali–alkali repulsion along the short a-axis. The short axis of antimonates under study (3.05–3.09 Å, see Table 1) is somewhat longer than that of titanates (2.93–2.99 Å [25–29]) and, thus, the repulsion effect is less significant. This result might be predicted: analysis of literature shows that, when Sb(5+) and Ti(4+) give rise to isostructural phases with octahedra sharing edges along the short axis of ca. 3 Å, this axis for antimony compounds is usually longer, often in contradiction with average ionic radii. Just one of dozens examples: rutile-type $AlSbO_4$, with cell volume 3% less than those for TiO_2, has 0.3% longer c-axis [21].

3.2. Superstructure models

As discussed previously [3,29], there are three known cation-ordered superlattice variants of the O3 type, $P3_112$, *C*2/*m* and *C*2/*c* (see Fig. 4), with very similar powder XRD patterns. Monoclinic phases $A_3Cu_2SbO_6$ (A=Li, Na) may be easily recognized due to strong Jahn–Teller distortions, but in other instances, monoclinic lattices are metrically similar to trigonal ones, as illustrated by parameters $b/a\sqrt{3}$ and $(-3c\cos\beta)/a$, close to unity [3], and do not show line splitting on powder patterns. Another characteristic feature of these phases is strong sloping background near the superlattice reflections, indicating stacking faults [34,35].

These features are also characteristic of the four $Na_3M_2SbO_6$ phases under study. In contrast to our indication that $Na_3Co_2SbO_6$ is trigonal [6–8], Cava et al. [9] refined it in space group *C*2/*m* by analogy with our $Na_3Cu_2SbO_6$ [3]. However, their neutron diffraction pattern measured with a 0.05° step does not show any splitting and they do not report any attempt to try a trigonal model. As evident from Table 2, their monoclinic lattice is even closer to the trigonal metrics than ours, indexed as trigonal with reasonably high figure of merit (FoM); on going to the monoclinic lattice, the FoM is slightly reduced and the lattice parameters only change within experimental errors (0.5–3 e.s.d.).

Of course, the lattice may remain monoclinic even when its metrics occasionally seems trigonal. This depends on the M/Sb ordering scheme (Fig. 4), which can only be resolved with superlattice reflections. However, these reflections are weak and their calculated intensities do not show significant changes on going from $P3_112$ to *C*2/*m* (see Fig. 1). In addition, it seems strange that, besides $Na_3M_2SbO_6$, the same "occasional coincidence" of metrics takes place for many other compounds [3].

Unambiguous discrimination between these types may only be achieved by observing diffraction line splitting, optical anisotropy or second harmonic generation ($P3_112$ phase should be uniaxial,

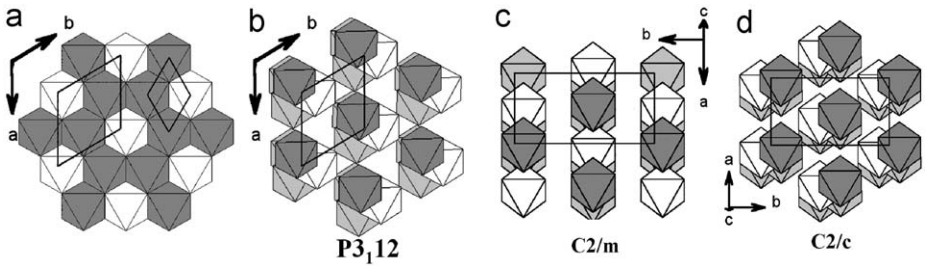

Fig. 4. A comparison of the three superlattice types derived from O3 (α-$NaFeO_2$ type) with general formula $A_3(M_2X)O6$. (a) An octahedral M_2XO_6 layer parallel to (001), common for all the three superlattice types. The supercell and subcell are outlined. The MO_6 and XO_6 octahedra are grey and white, respectively. (b), (c), (d) Arrangements of the XO_6 octahedra (A and M cations are omitted for clarity) in $Li_3(Li_2Re)O_6$, $P3_112$ [31], $Li_3(Zn_2Sb)O_6$, $C2/m$ [32] and $Li_3(Ti_2Li)O_6$, $C2/c$ [33], respectively. Different colours are used for identical XO_6 octahedra at different levels.

acentric, rotating polarization plane, whereas the monoclinic phases should be biaxial, centrosymmetrical and non-rotating). However, optical data are absent.

Intuitively, the most symmetrical of the two indistinguishable cases would seem more appropriate, but here we meet a dilemma. When indexing a powder pattern, the trigonal case is, undoubtedly, more symmetrical. But when refining the crystal structure, the $C2/m$ model with seven variable coordinates [9] is more symmetrical than the $P3_112$ model with fifteen variable coordinates, not to mention thermal parameters.

Cell metrics of $Na_3Ni_2SbO_6$ fits the trigonal system even better (Table 2). After exclusion of the 2Θ range 18–32° containing only superlattice reflections (Fig. 1a), its XRD pattern enables refinement within an ideal O3-type structure with reasonably low discrepancy indices of R_{F2}=3.58% and χ^2=3.77. Similar to $Na_3Co_2SbO_6$, the two variants of Ni/Sb ordering, $P3_112$ and $C2/m$ (Fig. 1b, c), provide equally reasonable explanation of the superlattice reflections but cannot account for the anomalous background and six additional extremely weak ($I<0.3\%$) reflections (four of them are marked with arrows in Fig. 1a), only indexable with semi-integer l values. This needs either doubling the hexagonal c axis or conversion to the $C2/c$ model (Fig. 1d).

It may be concluded that trigonal and monoclinic structures for the $Na_3M_2SbO_6$ compositions (together with many other $A_3M_2LO_6$ [3,29,34,35]) are very similar in both metrics and lattice energy and may coexist in a crystal creating stacking faults manifested by broadening of superlattice reflections and anomalous background between them.

3.3. Hydration

All the layered phases under study, both ordered and disordered, show two additional low-angle reflections with d-spacing ratio of 2 when stored off a desiccator in ambient air. Along with enhancement of these reflections, 003 and 006 peaks of the main phase weaken, whereas the rest of the pattern remains essentially the same. This indicates formation of a second trigonal phase with the same parameter a but increased c (up to 21.2 Å), obviously due to absorption of moisture into the interlayer. Similar but much more rapid processes were observed with structurally related potassium phases $K_xM_{(1+x)/3}Sb_{(2-x)/3}O_2$ (M=Ni, Co, Mg) [1]. However, they also showed reflections from $KHCO_3$, a product of exchange reaction with carbonic acid. To examine whether this reaction is responsible for the observed c-axis expansion, we stored two identical powdered samples of $Na_{0.8}Co_{0.6}Sb_{0.4}O_2$ in ordinary air and in a closed vessel over diluted aqueous solution of NaOH to absorb any CO_2. Results, shown in Fig. 5, demonstrate that the effect of moist CO_2-free air

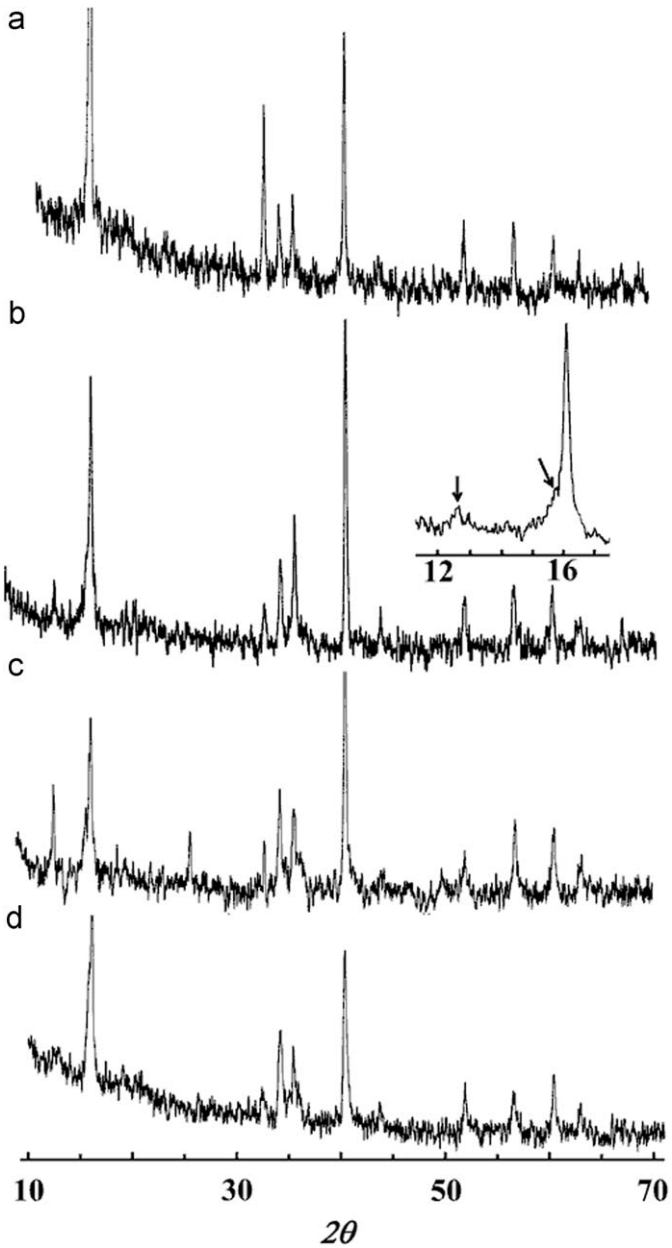

Fig. 5. XRD powder patterns of $Na_{0.8}Co_{0.6}Sb_{0.4}O_2$ in the course of hydration (a) As prepared; 00l reflections are enhanced due to grain orientation. (b) and (c) The same powder stored over NaOH solution for 10 and 24 days, respectively. Insert shows expanded low-angle range. First signs of hydration are marked with arrows. (d) The sample stored in ambient air for 24 days.

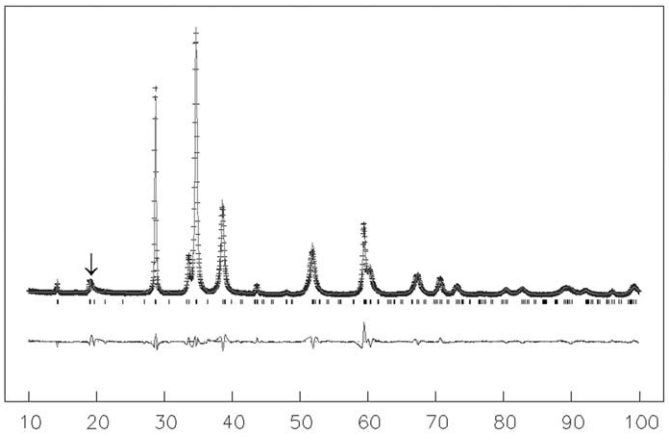

Fig. 6. X-ray diffraction pattern of $Ag_3Co_2SbO_6$. Crosses, experimental data; line, calculated profile; bottom, difference; vertical bars, Bragg positions. The arrow points to the sole superlattice reflection (100).

Table 3
Crystallographic data for $Ag_3Co_2SbO_6$ and details of structure refinement.

Crystal system	Trigonal
Space group	$P3_112$ (No.151)
Lattice constants	
a (Å)	5.3842(2)
c (Å)	18.6613(10)
Cell volume (Å^3)	468.51
Formula weight	659.2
Z	3
2θ range	10–100°
Number of data points	4500
Number of reflections	440
Number of parameters	62
Agreement factors	
R_p	4.22%
R_{F2}	5.07%
χ^2	3.71

Table 4
Atomic coordinates and thermal displacement parameters for $Ag_3Co_2SbO_6$.

Atom	Position	x	y	z	U_{iso}
Sb	3*a*	0.4579(6)	0.2290(3)	0	0.027(3)
Co_1	3*a*	0.1177(6)	0.5588(3)	0	0.021(9)
Co_2	3*a*	0.7801(8)	0.8900(4)	0	0.0032(5)
Ag_1	3*b*	0.1080(7)	−0.1080(7)	−1/6	0.0050(7)
Ag_2	3*b*	0.7762(8)	0.2238(8)	−1/6	0.026(3)
Ag_3	3*b*	0.4546(4)	−0.4546(4)	−1/6	0.016(3)
O_1	6*c*	0.1318(11)	0.2272(8)	0.06101(6)	0.0009(4)
O_2	6*c*	0.7828(13)	0.5272(9)	0.06054(7)	0.0021(9)
O_3	6*c*	0.4460(9)	0.9135(9)	0.06126(6)	0.0015(6)

is much stronger and, therefore, the *c*-axis expansion is only due to absorption of water and does not need CO_2.

3.4. Ion-exchange reaction and crystal structure of $Ag_3Co_2SbO_6$

Ion exchange is the simplest and most direct indication of ion mobility in a crystal. Besides this, it allows preparation of new phases which, in many instances, cannot be prepared by direct synthesis. As an example, we tried silver ion exchange in $Na_3Co_2SbO_6$. The powder was mixed with double excess of silver nitrate, heated to 260 °C (slightly above the melting point of $AgNO_3$ and near the liquidus temperature of the expected product, $Na_{0.5}Ag_{0.5}NO_3$), kept for an hour, cooled, washed with water and dried. Thus prepared reddish-brown powder contains 47.3 wt% Ag (calculated for $Ag_3Co_2SbO_6$, 49.3%). Its XRD pattern (Fig. 6) is typical of the delafossite-type phases but, similarly to its sodium precursor, contains a superlattice reflection indicating tripling of the unit-cell volume. Relative intensity of the superlattice effects is decreased because the main scatterer is now silver, only contributing to the sublattice reflections. A starting structural model was easily built from the $P3_112$ model of $Na_3(NaFeSb)O_6$ [2] or $Na_3(LiTi_2)O_6$ [29] by mere changing sign of the *z* coordinate of oxygen atoms to provide linear coordination for silver instead of octahedral coordination for sodium. This is exactly the same as transformation of α-$NaFeO_2$ to delafossite. Of course, the real transformation during ion-exchange occurs by layer gliding rather than this "mirror inversion". The model was successfully refined to reasonably low values of R and χ^2 (Table 3). The resulting structural parameters and bond lengths are listed in Tables 4, 5, and the structure is shown in Fig. 7, together with the sodium precursor. It might be seen that the average Sb–O and Co_2–O bond lengths are somewhat longer, and Ag–O bond lengths are somewhat shorter than the corresponding sums of radii. We do not think that these differences are significant. Most probably, they result from low accuracy in location of oxygen, the lightest element compared to heavy Ag, Sb and Co.

$Ag_3Co_2SbO_6$ is, apparently, the first structurally characterized cation-ordered silver delafossite. Analogous compositions, $Ag_3M_2SbO_6$ (*M*=Ni, Zn), prepared similarly from their lithium counterparts, did not show superlattice reflections and were indexed in small delafossite-type cells although the authors emphasized high probability of the cation ordering [37]. On the other hand, $Ag_3LiTi_2O_6$ [29] and $Ag_3NaFeSbO_6$ [2] do exhibit superlattice effects (a=5.22–5.45 Å; c=18.57–18.77 Å) but their structures have not been refined.

Lithium exchange reactions have also been successfully performed and the results will be reported elsewhere.

3.5. Ionic conductivity

For electrical measurements, we selected the Ni-containing material which seemed most interesting due to the shortest *a*-axis value and highest electronegativity of M(2+), both factors being favourable for Na-ion conduction. As can be seen from Fig. 8, conductivity values of our sample are considerably greater than

Table 5
Bond lengths in $Ag_3Co_2SbO_6$ (Å).

	Sb–O_3	2.022(8) × 2	Co_1–O_2	2.061(9) × 2	Co_2–O_1	2.177(8) × 2	Ag_1–O_1	1.975(11) × 2
	Sb–O_2	2.026(9) × 2	Co_1–O_1	2.151(8) × 2	Co_2–O_3	2.188(7) × 2	Ag_2–O_2	1.988(13) × 2
	Sb–O_1	2.088(8) × 2	Co_1–O_3	2.169(8) × 2	Co_2–O_2	2.263(9) × 2	Ag_3–O_3	1.968(11) × 2
Average		2.045		2.127		2.209		1.977
Radii sum [24]		1.98		2.125				2.05

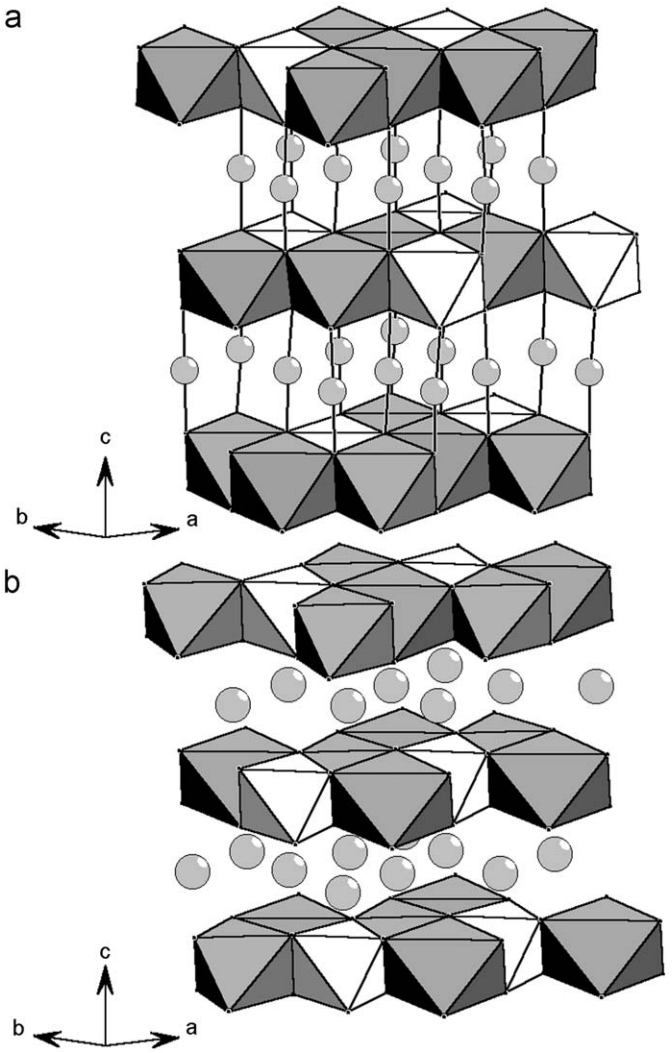

Fig. 7. Crystal structure of $Ag_3Co_2SbO_6$ (a) and starting $Na_3Co_2SbO_6$ (b). White octahedra, SbO_6; grey octahedra, CoO_6; circles, Ag^+ or Na^+.

reported earlier for the same composition [4]. We attribute this difference mostly to the grain orientation in our sample prepared by the uniaxial hot pressing and measured in the direction perpendicular to the pressure direction, i.e., parallel to the conduction layers. Nevertheless, these values are somewhat lower than those for isostructural phases with the same sodium contents: $Na_{0.8}Fe_{0.8}Ti_{0.2}O_2$ [38] and $Na_{0.8}Fe_{0.9}Sb_{0.1}O_2$ [2]. Again, we explain these results by shorter *a*-axis values of the two iron compounds, 3.00 and 3.02 Å, respectively, vs. 3.05 Å for the nickel compound.

4. Conclusions

All the four Na_2O–*M*O–SbO_y systems (*M*=Ni, Co, Zn, Mg) contain both disordered (sodium-deficient) and cation-ordered (completely filled) α-$NaFeO_2$-type phases. The ordering in $Na_3M_2SbO_6$ is accompanied by stacking faults which preclude unambiguous distinction between the trigonal and monoclinic superlattices. Sodium cation mobility in these phases is demonstrated by ionic conductivity of $Na_{0.8}Ni_{0.6}Sb_{0.4}O_2$ ceramics and ion-exchange preparation of $Ag_3Co_2SbO_6$, the first structurally characterized cation-ordered silver delafossite. The sodium compounds should be protected from moisture since they are

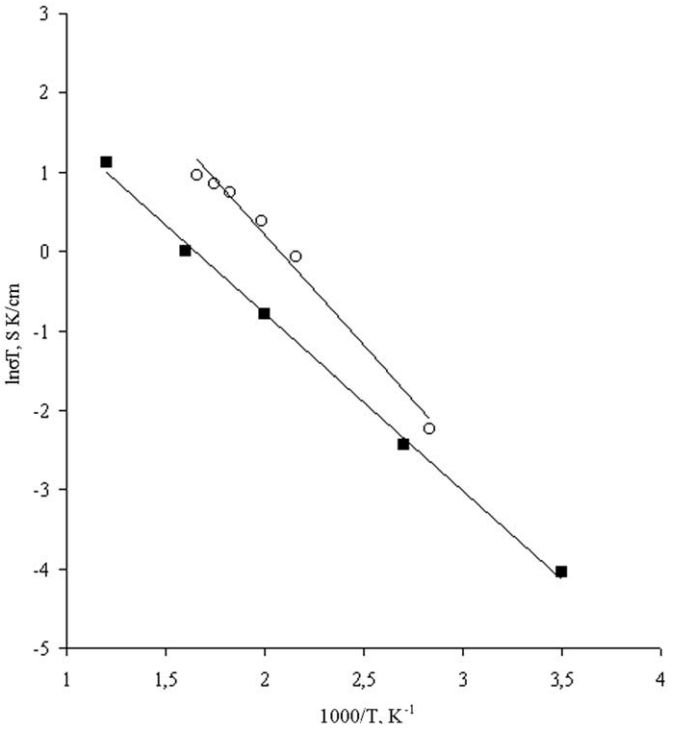

Fig. 8. Temperature dependence of conductivity of $Na_{0.8}Ni_{0.6}Sb_{0.4}O_2$ ceramics obtained in the present work (open circles) and in Ref. [4] (filled squares).

able to intercalate water from the atmosphere with *c*-axis expansion up to 29% which may be detrimental for the ceramics.

Acknowledgements

The work was supported by internal Grant K-07-T-20 of the South Federal University, Grants 97-03-33807 and 00-03-32469 from the Russian Foundation for Basic Research and Grant-in-aid 00-15 from the International Centre for Diffraction Data. The authors thank Dr. O.A. Smirnova who prepared the most pure sample of $Na_3Ni_2SbO_6$, Drs M. Avdeev and S.N. Polyakov for the Rigaku scans.

Appendix A. Supplementary material

Supplementary data associated with this article can be found in the online version at doi:10.1016/j.jssc.2009.12.002.

References

[1] O.A. Smirnova, V.B. Nalbandyan, M. Avdeev, L.I. Medvedeva, B.S. Medvedev, V.V. Kharton, F.M.B. Marques, J. Solid State Chem. 178 (2005) 172.
[2] V.V. Politaev, V.B. Nalbandyan, Solid State Sci. 11 (2009) 144.
[3] O.A. Smirnova, V.B. Nalbandyan, A.A. Petrenko, M. Avdeev, J. Solid State Chem. 178 (2005) 1165.
[4] O.A. Smirnova, R.O. Fuentes, F. Figueiredo, V.V. Kharton, F.M.B. Marques, J. Electroceram. 11 (2003) 179.
[5] O.A. Smirnova, M. Avdeev, V.B. Nalbandyan, V.V. Kharton, F.M.B. Marques, Mater. Res. Bull. 41 (2006) 1056.
[6] V.B. Nalbandyan, I.L. Shukaev, V.V. Politaev, V.A. Volotchaev, L.I. Medvedeva, B.S. Medvedev, O.A. Smirnova, in: II National Crystal Chemical Conference Abstracts of Papers, Chernogolovka, Moscow oblast, Russia, 23–26 May 2000, p. 183 (In Russian).
[7] O.A. Smirnova, V.B. Nalbandyan, V.V. Politaev, L.I. Medvedeva, V.A. Volotchaev, I.L. Shukaev, B.S. Medvedev, A.A. Petrenko, in: P. Bezdicka and T. Grygar (Ed.), Solid State Chemistry 2000, Academy of Sciences of the Czech Republic, Prague, 2000, p. 228.

[8] O.A. Smirnova, V.B. Nalbandyan, V.V. Politaev, V.A. Volotchaev, I.L. Shukaev, L.I. Medvedeva, B.S. Medvedev, A.A. Petrenko, in: XII Russian Conference on Physical Chemistry and Electrochemistry of Molten and Solid Electrolytes, vol. 2, Naltchik, Russia, 2001, p. 102 (In Russian).
[9] L. Viciu, Q. Huang, E. Morosan, H.W. Zandbergen, N.I. Greenbaum, T. McQueen, R.J. Cava, J. Solid State Chem. 180 (2007) 1060.
[10] Y. Miura, R. Hirai, T. Fujita, Y. Kobayashi, M. Sato, J. Magn. Magn. Phenom. 310 (2) (2007) e389.
[11] S. Derakhshan, H.L. Cuthbert, J.E. Greedan, B. Rahaman, T. Saha-Dasgupta, Phys. Rev. B 76 (2007) 104403.
[12] B. Schwedes, R. Hoppe, Z. Anorg. Allg. Chem. 393 (1972) 136.
[13] B. Wang, S.C. Chen, M. Greenblatt, J. Solid State Chem. 108 (1994) 184.
[14] G.M. Kale, S. Srikanth, J. Am. Ceram. Soc. 82 (1999) 2161.
[15] G. Bayer, Naturwissenschaften 48 (1961) 46.
[16] H. Kasper, Z. Kristallogr. 128 (1969) 72.
[17] J.N. Reimers, J.E. Greedan, C.V. Stager, R. Kremer, J. Solid State Chem. 83 (1989) 20.
[18] E. Ramos, F. Fernandez, A. Jerez, C. Pico, J. Rodriguez-Carvajal, R. Saez-Puche, M.L. Veiga, Mater. Res. Bull. 27 (1992) 1041.
[19] K. Swaminathan, O.M. Sreedharan, J. Alloys Compds. 292 (1999) 100.
[20] G.C. Miles, A.R. West, J. Am. Ceram. Soc. 88 (2005) 396.
[21] Powder Diffraction File, International Centre for Diffraction Data, 2007.
[22] A.C. Larson, R.B. VonDreele, General Structure Analysis System (GSAS), Los Alamos National Laboratory Report LAUR 86-748 (2004).
[23] B.H. Toby, J. Appl. Cryst. 34 (2001) 210.
[24] R.D. Shannon, Acta Cryst. A 32 (1976) 751.
[25] V.B. Nalbandyan, I.L. Shukaev, Russ. J. Inorg. Chem. 37 (1992) 1231.
[26] I.L. Shukaev, V.A. Volochaev, Russ. J. Inorg. Chem. 40 (1995) 1974.
[27] M.Y. Avdeev, V.B. Nalbandyan, B.S. Medvedev, Inorg. Mater. (1997) 500.
[28] G.V. Shilov, V.B. Nalbandyan, V.A. Volochaev, L.O. Atovmyan, Int. J. Inorg. Mater. 2 (2000) 443.
[29] V.B. Nalbandyan, Russ. J. Inorg. Chem. 45 (2000) 1652.
[30] C. Delmas, C. Fouassier, P. Hagenmuller, Mater. Res. Bull. 11 (1976) 1483.
[31] J. Hauck, Z. Naturforschung B 23 (1968) 1603.
[32] C. Greaves, S.M.A. Katib, Mater. Res. Bull. 25 (1990) 1175.
[33] J.F. Dorrian, R.E. Newnham, Mater. Res. Bull. 4 (1969) 179.
[34] M. Trömel, J. Hauck, Z. Anorg. Allg. Chem. 373 (1970) 8.
[35] J.M. Paulsen, R.A. Donaberger, J.R. Dahn, Chem. Mater. 12 (2000) 2257.
[36] G.S. Smith, R.L. Snyder, J. Appl. Cryst. 12 (1979) 60.
[37] R. Nagarajan, S. Uma, M.K. Jayaraj, J. Tate, A.W. Sleight, Solid State Sci. 4 (2002) 787.
[38] E.I. Burmakin, G.Sh. Shekhtman, Elektrokhimiya 21 (1985) 752 (In Russian).